CCFE-PR(17)57

Kazuto Arakawa, Mihai-Cosmin Marinica, Steven Fitzgerald,
Laurent Proville, Duc Nguyen-Manh, Sergei L. Dudarev,
Pui-Wai Ma, Thomas D. Swinburne, Tetsuya Yamada,
Takafumi Amino, Shigeo Arai, Yuta Yamamoto, Kimitaka Higuchi,
Nobuo Tanaka, Hidehiro Yasuda, Tetsuya Yasuda, Hirotaro Mori

Observation of quantum-assisted transport of heavy defects in tungsten

Observation of quantum-assisted transport of heavy defects in tungsten

Kazuto Arakawa[1], Mihai-Cosmin Marinica[2], Steven Fitzgerald[3], Laurent Proville[2], Duc Nguyen-Manh[4], Sergei L. Dudarev[4], Pui-Wai Ma[4], Thomas D. Swinburne[5], Tetsuya Yamada[6], Takafumi Amino[7], Shigeo Arai[8], Yuta Yamamoto[8], Kimitaka Higuchi[8], Nobuo Tanaka[8], Hidehiro Yasuda[9], Tetsuya Yasuda[9], Hirotaro Mori[9]

[1]Department of Materials Science, Faculty of Science and Engineering, Shimane University, 1060 Nishikawatsu, Matsue 690-8504, Japan.
[2]DEN-Service de Recherches de Métallurgie Physique, CEA, Université Paris-Saclay, F-91191, Gif-sur-Yvette, France.
[3]Department of Applied Mathematics, University of Leeds, Leeds LS2 9JT, UK
[4]Culham Centre for Fusion Energy, Culham Science Centre, Abingdon, Oxfordshire, OX14 3DB, United Kingdom.
[5]Theoretical Division T-1, Los Alamos National Laboratory, Los Alamos, New Mexico, 87545, USA.
[6]Railway, Automotive & Machinery Parts Unit Osaka Steel Works, Nippon Steel & Sumitomo Metal Corporation, 1-109, Shimaya 5-chome, Konohana-ku, Osaka 554-0024, Japan.
[7]Advanced Technology Research Laboratories, Nippon Steel & Sumitomo Metal Corporation, 1-8 Fuso-Cho, Amagasaki, Hyogo 660-0891, Japan.
[8]Institute of Materials and Systems for Sustainability, Nagoya University, Nagoya 464-8603, Japan.
[9]Research Centre for Ultra-High Voltage Electron Microscopy, Osaka University, 7-1 Mihogaoka, Ibaraki, Osaka 567-0047, Japan.

Observation of quantum-assisted transport of heavy defects in tungsten

Kazuto Arakawa[1], Mihai-Cosmin Marinica[2], Steven Fitzgerald[3], Laurent Proville[2], Duc Nguyen-Manh[4], Sergei L. Dudarev[4], Pui-Wai Ma[4], Thomas D. Swinburne[5], Tetsuya Yamada[6], Takafumi Amino[7], Shigeo Arai[8], Yuta Yamamoto[8], Kimitaka Higuchi[8], Nobuo Tanaka[8], Hidehiro Yasuda[9], Tetsuya Yasuda[9], Hirotaro Mori[9]

[1]*Department of Materials Science, Faculty of Science and Engineering, Shimane University, 1060 Nishikawatsu, Matsue 690-8504, Japan.*

[2]*DEN-Service de Recherches de Métallurgie Physique, CEA, Université Paris-Saclay, F-91191, Gif-sur-Yvette, France.*

[3]*Department of Applied Mathematics, University of Leeds, Leeds LS2 9JT, UK*

[4]*Culham Centre for Fusion Energy, Culham Science Centre, Abingdon, Oxfordshire OX14 3DB, United Kingdom.*

[5]*Theoretical Division T-1, Los Alamos National Laboratory, Los Alamos, New Mexico, 87545, USA.*

[6]*Railway, Automotive & Machinery Parts Unit Osaka Steel Works, Nippon Steel & Sumitomo Metal Corporation, 1-109, Shimaya 5-chome, Konohana-ku, Osaka 554-0024, Japan.*

[7]*Advanced Technology Research Laboratories, Nippon Steel & Sumitomo Metal Corporation, 1-8 Fuso-Cho, Amagasaki, Hyogo 660-0891, Japan.*

[8]*Institute of Materials and Systems for Sustainability, Nagoya University, Nagoya 464-8603, Japan.*

[9]*Research Centre for Ultra-High Voltage Electron Microscopy, Osaka University, 7-1 Mihogaoka, Ibaraki, Osaka 567-0047, Japan.*

Quantum dynamics within solids is usually restricted to low mass particles such as electrons and muons, or single atoms of light elements such as hydrogen[1,2]. In this Letter we report observation of the quantum-assisted motion of self-interstitial atom clusters in tungsten (each of mass 184 Da), travelling distances of several nanometres between trapping points associated with impurity atoms or vacancies. This is the first direct experimental observation of quantum diffusion at low temperatures in a high-voltage electron microscope (HVEM). The underlying reasons behind the process are the non-equilibrium effects of electron irradiation, which we exploit to reduce the effective trap depth by several orders of magnitude, and the emergence of the clusters as delocalized quasiparticles that, once escaped, can move almost unimpeded through the crystal. The stochastic cluster motion is driven by quantized atomic vibrations, and involves the collective dynamics of more than the 100 or so atoms forming each cluster. This coherent behaviour leads to low temperature diffusion rates orders of magnitude higher than a naive classical estimate suggests. Our results demonstrate the importance of quantum effects on low temperature defect evolution even in heavy atom systems, and underline the invalidity of the standard Arrhenius form for diffusion rates, under these technologically important conditions. Our analysis shows that this phenomenon is generic to any crystal, and can hence affect low temperature defect transport in almost any material.

Under high-energy irradiation (or extreme mechanical deformation), atoms in a crystal can be displaced significantly from their lattice positions, forming vacancy and self-interstitial atom (SIA) defects. These are ultimately responsible for severe degradation in the mechanical properties of nuclear materials, such as hardening,

swelling, and embrittlement[3]. Understanding the basic mechanisms controlling their formation and diffusion[4-6] is critical for the development of future next-generation energy systems.

In the field of material science, to the best of our knowledge, all observed migration processes of species heavier than H or He have been interpreted as thermal activation characterized by the Arrhenius rate[7], or phonon dragging[8,9]; no apparent quantum effects have been detected[10], although they have been theoretically considered for SIAs[11,12] and screw dislocations[13]. Quantum effects have also been observed on metal surfaces[14]. We focus here on the low temperature diffusion of SIA clusters in tungsten as a model for crystal defects in heavy-atom systems.

The lowest-energy SIA configuration in tungsten (and the other non-magnetic body-centred-cubic (bcc) transition metals) is the ⟨111⟩ crowdion, in which atomic displacements are confined almost entirely to the ⟨111⟩ string containing the extra atom. The defect is delocalized: it involves many more than one atom, as the displacement field is spread down the string, resulting in very low barriers to translation (known as *Peierls* barriers, see Supplementary Discussion 1). Hence crowdions perform one-dimensional (1D) diffusion along their axis with a low (meV scale) activation energy[8,15,16]. Similarly to single crowdions, SIA clusters in the form of $\mathbf{b} = \frac{1}{2}\langle 111 \rangle$ dislocation loops undergo 1D glide diffusion in the direction of **b**. This phenomenon has been studied using classical molecular dynamics simulations (MD)[17-21] and transmission electron microscopy (TEM)[5,22] for α-iron and other metals and alloys.

According to MD studies, the activation energy (Peierls barrier) for cluster diffusion is less than 0.1 eV[17,19], meaning they are thermally mobile even at very low temperatures. In any real material however, impurity atoms (mainly carbon and nitrogen) act as traps by binding to the clusters. Vacancies (expected at high density under irradiation) will mutually annihilate with SIAs at the cluster boundary, but can bind to the cluster's interior, and also act as traps.

Previous studies, using resistivity recovery and internal friction experiments[7], have shown that low-temperature cluster migration in tungsten (and other bcc metals) is strongly influenced by the concentration of impurity atoms and vacancies[23-25].

These traps are deep enough (~0.5 and 1 eV for vacancies and impurities respectively, see Supplementary Discussion 1) to prevent TEM observation of the clusters' thermal escape and subsequent motion on experimental timescales, even at 300 K, and they remain immobile. To overcome this, we used the HVEM's electron beam to enhance the vacancy mobility and reduce the effective trap depth. In the absence of the electron beam, vacancies are immobile up to 620-900 K[7], but in our experiment, the momentum imparted by the incident electrons moves the vacancies up to 100 times per second (see Supplementary Discussion 2). The experimental system is shown schematically in Fig. 1, and operates as follows.

First, a high energy (2000 keV) electron beam is used to create displacement damage, vacancies and SIAs at 105 K, before aging at 300 K. This allows the SIA clusters to nucleate and grow to the nanoscale, bound to impurities at their perimeters (where the binding energy is greatest). At these temperatures the vacancies are immobile and

remain dispersed throughout the sample. A lower energy (100-1000 keV) beam is then turned on the sample. These energies are too low to create additional vacancies and SIAs, but high enough to move the existing vacancies (see Methods and Supplementary Discussion 2), and the previously trapped clusters begin to move (Fig. 1; Supplementary Video 1). The key features of the motion are:

i) hops are rare events, i.e. the clusters spend far more time trapped than travelling between traps;
ii) clusters sometimes move back and forth between fixed points in the sample;
iii) clusters are observed to shrink under the beam;
iv) motion frequency depends strongly on temperature.

i) and ii) tell us that the clusters are escaping from the impurity traps, moving quickly through the lattice before being subsequently trapped again (a purely vacancy-based mechanism may also be possible; see Supplementary Discussion 2); iii) tells us how: the radiation-mobilized vacancies move through the crystal, attracted to the high compressive strain at the cluster boundaries. Here they annihilate the SIAs at the cluster boundaries, shrinking the cluster, and increasing the separation between the impurity atom and the cluster boundary. The impurity-cluster interaction is strong but short-ranged (see Supplementary Discussion 1), and falls off towards zero within a few lattice spacings, so the traps are now much shallower, and escape is easier (Fig. 1). We now turn to the temperature dependence, iv), which demonstrates that the low temperature escapes are quantum mechanical in nature.

Figure 2 is an Arrhenius plot showing the logarithm of the motion frequency vs. the inverse temperature. Hops due to thermal escape from potential wells of depth $\Delta V \ll k_B T$ have a characteristic rate $\propto \exp -\Delta V/k_B T$, i.e. a straight line on an

Arrhenius plot. This appears to be the case for the higher temperatures $T \geq 50$ K and the slope suggests ΔV is higher than 10 meV. As the temperature is reduced, 17 K $\leq T \leq$ 50 K, the slope flattens as the mechanism transitions from classical thermal escape towards temperature-independent quantum mechanical diffusion.

The measured rates result from three independent processes: the athermal radiation-driven vacancy migration under the beam (rate Γ_{vac}), the fluctuation-driven escape of the cluster from the trap (depth ΔV_{trap}, rate Γ_{trap}), and finally the traversal of the Peierls barrier intrinsic to the crystal (depth ΔV_P, rate Γ_P).

Figure 2 shows attempted classical fits for all barriers $10\text{meV} \leq \Delta V = \Delta V_P + \Delta V_{trap} \leq 90\text{meV}$. Note that the Peierls traversal rate is non-Arrhenius (since ΔV_P is not more than $k_B T$, see Methods), but no possible classical form for the rate can explain the observed values. (We are confident that the sample temperatures continue to decrease below 50 K, and are not significantly increased by beam heating – see Supplementary Discussion 3).

Figure 3 shows the same data points as Fig. 2, but this time with a quantum mechanical form for the escape rate Γ^{QM}, derived from the quantized nature of the crystal phonons (see Methods). These obey the Bose-Einstein rather than the Boltzmann statistics, and their zero-point fluctuations increase the average energy available for the cluster to overcome the barrier, thus increasing the low temperature rates in excellent agreement with the experimental values.

153 However, we still obtain acceptable fits for all barriers between 10 and 90meV. To
154 narrow this down, we considered the critical temperature T_c below which classical
155 physics breaks down (see Methods), which depends on the barrier height: Fig. 2
156 shows the 90 meV fit clearly failing below 140 K, whereas the 10 meV one appears
157 reasonable down to around 50 K. T_c depends on the phonon density of states, and is
158 estimated[26] to be 101 K for pure tungsten (about 1/3 of the Debye temperature). Fitted
159 values for T_c are also shown in Fig. 3, and the value 101 K is consistent with a barrier
160 height of 30 – 44 meV. We note that the resistivity recovery and internal friction
161 experiments cited earlier obtain a barrier height of 15 – 60 meV.
162
163 Other manifestations of quantum behaviour are in principle possible, in particular the
164 deep tunneling of the entire cluster. However, fitting the data to this functional form
165 requires unrealistic values for cluster's effective mass (see Methods), and we
166 conclude that, over the range of temperatures probed by our experiment, quantized
167 phonons facilitating the clusters' escape from traps 30 – 44 meV deep provide the
168 optimal model explaining the data.
169
170 In this study we have performed the first direct investigation of cryogenic defect
171 diffusion in the electron microscope. Our unique experimental system allowed us to
172 manipulate the effective potential wells encountered by SIA clusters, reducing their
173 depth until we could probe the quantum mechanical nature of their diffusion. We
174 conclude that below around 1/3 of the Debye temperature, quantum atomic vibration
175 effects become important. Moreover, the behaviour derives from quantized phonons,
176 which drive the stochastic fluctuations of objects that are themselves too heavy to

tunnel significantly. This likely affects low temperature defect transport in many crystalline materials.

References

1 Kadono, R. *et al.* Quantum diffusion of positive muons in copper. *Physical Review B* **39**, 23-41 (1989).

2 Sundell, P. G. & Wahnström, G. Activation energies for quantum diffusion of hydrogen in metals and on metal surfaces using delocalized nuclei within the density-functional theory. *Physical Review Letters* **92**, 155901 (2004).

3 Gary, S. W. *Fundamentals of radiation Materials Science*. (Springer, 2007).

4 Fu, C.-C., Torre, J. D., Willaime, F., Bocquet, J.-L. & Barbu, A. Multiscale modelling of defect kinetics in irradiated iron. *Nature Materials* **4**, 68-74 (2005).

5 Arakawa, K. *et al.* Observation of the one-dimensional diffusion of nanometer-sized dislocation loops. *Science* **318**, 956-959, doi:10.1126/science.1145386 (2007).

6 Bai, X.-M., Voter, A. F., Hoagland, R. G., Nastasi, M. & Uberuaga, B. P. Efficient Annealing of Radiation Damage Near Grain Boundaries via Interstitial Emission. *Science* **327**, 1631-1634, doi:10.1126/science.1183723 (2010).

7 Ehrhart, P., Jung, P., Schultz, H. & Ullmaier, H. *Atomic Defects in Metals*. Vol. 25 (Springer-Verlag, Berlin, 1991).

8 Derlet, P. M., Nguyen-Manh, D. & Dudarev, S. L. Multiscale modeling of crowdion and vacancy defects in body-centered-cubic transition metals. *Physical Review B* **76**, 054107 (2007).

9 Swinburne, T. D., Dudarev, S. L. & Sutton, A. P. Classical Mobility of Highly Mobile Crystal Defects. *Physical Review Letters* **113**, 215501 (2014).

10 Wollenberger, H. J. in *Physical Metallurgy, Part II* (eds R. W. Chan & P. Haasen) 1139 (North Holland Physics Publishing, Amsterdam, 1983).

11 Pushkarov, D. I. Quantum theory of crowdions at low temperatures. *Soviet Journal of Experimental and Theoretical Physics* **37** (1973).

12 Flynn, C. P. Resonance mode hopping and the stage I annealing of metals. *Thin Solid Films* **25**, 37-43, doi:http://dx.doi.org/10.1016/0040-6090(75)90242-4 (1975).

13 Proville, L., Rodney, D. & Marinica, M.-C. Quantum effect on thermally activated glide of dislocations. *Nat Mater* **11**, 845-849, doi:http://www.nature.com/nmat/journal/v11/n10/abs/nmat3401.html#supplementary-information (2012).

14 Ohresser, P. *et al.* Surface Diffusion of Cr Adatoms on Au(111) by Quantum Tunneling. *Physical Review Letters* **95**, 195901 (2005).

15 Fitzgerald, S. P. & Nguyen-Manh, D. Peierls potential for crowdions in the bcc transition metals. *Physical Review Letters* **101**, 115504 (2008).

16 Amino, T., Arakawa, K. & Mori, H. Detection of one-dimensional migration of single self-interstitial atoms in tungsten using high-voltage electron microscopy. *Sci Rep* **6**, 26099, doi:10.1038/srep26099 (2016).

17 Wirth, B. D., Odette, G. R., Maroudas, D. & Lucas, G. E. Dislocation loop structure, energy and mobility of self-interstitial atom clusters in bcc iron. *J Nucl Mater* **276**, 33-40, doi:http://dx.doi.org/10.1016/S0022-3115(99)00166-X (2000).
18 Marian, J. *et al.* Dynamics of self-interstitial cluster migration in pure α-Fe and Fe-Cu alloys. *Physical Review B* **65**, 144102 (2002).
19 Osetsky, Y. N., Bacon, D. J., Serra, A., Singh, B. N. & Golubov, S. I. One-dimensional atomic transport by clusters of self-interstitial atoms in iron and copper. *Philos Mag* **83**, 61-91, doi:10.1080/0141861021000016793 (2003).
20 Dudarev, S. L. The non-Arrhenius migration of interstitial defects in bcc transition metals. *Comptes Rendus Physique* **9**, 409-417, doi:10.1016/j.crhy.2007.09.019 (2008).
21 Swinburne, T. D., Dudarev, S. L., Fitzgerald, S. P., Gilbert, M. R. & Sutton, A. P. Theory and simulation of the diffusion of kinks on dislocations in bcc metals. *Physical Review B* **87**, 064108 (2013).
22 Arakawa, K., Amino, T. & Mori, H. One-dimensional glide motion of "naked" 1/2<111> prismatic dislocation loops in iron. *ISIJ International* **54**, 2421-2424 (2014).
23 Dausinger, F. & Schultz, H. Long-range migration of self-interstitial atoms in tungsten. *Physical Review Letters* **35**, 1773-1775 (1975).
24 Dausinger, V. F. Die Tieftemperaturerholung in elektronenbestrahltem Wolfram. *Philosophical Magazine A* **37**, 819-836, doi:10.1080/01418617808239211 (1978).
25 Mizubayashi, H. & Okuda, S. Elastic after-effect studies of self-interstitials in tungsten after fast neutron irradiation at 5 K. *Radiation Effects* **54**, 201-215, doi:10.1080/00337578108210049 (1981).
26 Ashcroft, N. W. & Mermin, N. D. *Solid State Physics*. (College Edition, New York, 1978).

Supplementary Information accompanies the paper on **www.nature.com/nature**.

Acknowledgements This work was financially supported by Grants-in-Aid for Scientific Research (Grant No. 15H04244, and 15K14109) from Japan Society for the Promotion of Science, and the Iron and Steel Institute of Japan Research Promotion Grant. Part of this work was supported by the "Advanced Characterization Nanotechnology Platform, Nanotechnology Platform Programs" of the Ministry of Education, Culture, Sports, Science and Technology (MEXT), Japan, at Institute of Materials and Systems for Sustainability (Nanotechnology Open Facilities) in Nagoya University and at Research Centre for Ultra-High Voltage Electron Microscopy (Nanotechnology Open Facilities) in Osaka University, and TATARA Nanotechnology Project Centre in Shimane University. M.C.M. acknowledges support from the GENCI -(CINES/CCRT) computer centre under Grant No. A0010906973. The work at CCFE has been carried out within the framework of the EUROfusion Consortium and has received funding from the Euratom research and training programme 2014-2018 under grant agreement No 633053 and funding from the RCUK Energy Programme [grant number

EP/P012450/1]. The views and opinions expressed herein do not necessarily reflect those of the European Commission.

Authors Contributions K.A., M.C.M. and L.P. designed the study. K.A., T.Y., T.A., S.A., Y.Y., K.H., S.M., N.T., H.Y., T.Y. and H.M. performed the experiments. M.C.M., S.F., L.P., D.N.M., S.L.D., P.W.M. and T.D.S. performed the theoretical works. K.A., M.C.M., S.F., and S.L.D. wrote the main draft. All authors discussed the results and commented on the manuscript.

Author Information Reprints and permission information is available at www.nature.com/reprints. Correspondence and requests for materials should be addressed to K.A. (arakawa@riko.shimane-u.ac.jp).

METHODS

Specimen preparation We cut (011) discs from one grain of an ingot of high-purity coarse-grained polycrystalline tungsten (99.9999 mass % JX Nippon Mining & Metals Co., Tokyo, Japan; impurity amounts of the ingot are given in Ref. [27]). The discs were thinned to 0.1mm, using spark erosion and mechanical polishing, then perforated at the centre by electropolishing so the periphery of the hole became cross-sectionally wedge-shaped for TEM observations.

Production of SIA clusters We used high-energy electron irradiation in a HVEM (Hitachi H-3000) to create SIAs and vacancies in the thin foil specimens. The acceleration voltage was 2000 kV, and a temperature of 105 K was maintained using a liquid-nitrogen-cooled specimen holder (Oxford Instruments). We note that the thermal migration of vacancies is frozen at temperatures below 620-900 K[7]. The beam flux was 1×10^{24} $m^{-2}s^{-1}$, and the dose was 4×10^{25} m^{-2}.

During 2000-keV electron irradiation, pairs of SIAs and vacancies are produced[28] via knock-on displacement. Based on our recent work[16,27], the point defect reactions proceed as follows: most of the highly mobile 1D-moving SIAs react with vacancies, or escape to the foil surface, where they are annihilated. Surviving SIAs bind to impurity atoms and form embryonic SIA clusters, that grow by absorbing other SIAs, and take the form of $\mathbf{b} = \frac{1}{2}\langle 111 \rangle$ dislocation loops. These clusters are intrinsically highly mobile, yet they are trapped by impurities and remain stationary. Vacancies that do not react with SIAs accumulate throughout the irradiated area of the specimen.

Using TEM, the average size and density of the SIA formed clusters under the above condition were found to be approximately 3-4 nm and 4×10^{22} m^{-3}, respectively. Accumulated vacancies are not visible in the TEM. After the irradiation, the specimen was aged at approximately 300 K. This allows the clusters trapped by weak impurity atoms with shallow potential wells to thermally escape and move, leading to coalescence with other clusters[29], escape to the specimen surfaces, or to trapping by stronger impurities with deeper wells. However, even after aging for several months, we did not see any significant change in the cluster density, demonstrating that thermal escape of SIA clusters from the deeper wells hardly occurs even at 300 K.

TEM observation of the 1D motion of SIA clusters in response to high-energy electron irradiation We then used the electron beam to enhance the vacancy mobility (see main text and Supplementary Discussion 2), with acceleration voltages of 100, 150, 300, 500 (Hitachi H-9000UHV), 1000, and 2000kV (H-3000) – all

except 2000kV are below the threshold for point defect generation in tungsten[28]. Additional very intense irradiations were carried out at 1000kV using a JEOL JEM 1000K RS. Beam fluxes ranged from 5×10^{22} to 2×10^{25} $m^{-2}s^{-1}$, and temperatures ranged from 17-300 K (where no thermal migration of vacancies takes place[7]). We achieved these temperatures using liquid-helium-cooled specimen holders (Oxford Instruments), in which the temperature is measured with a thermocouple attached to the specimen mount, so the measured temperature is the average over the whole specimen.

The specimen thickness ranged from 50 to 70 nm (measured using equal-thickness fringes[30]). The observations were carried out using the weak-beam dark-field technique[31] with a reflection of **g** = 200. Under this condition, all SIA clusters in the form of prismatic dislocation loops with a **b** = ½⟨111⟩ type Burgers vector and a diameter greater than approximately 2 nm were imaged. The dynamic response of the clusters was monitored and recorded with CCDs having frame rates of 30 fps for H-9000UHV and H-3000, and 15 fps for JEM 1000K RS.

We define the motion frequency of the clusters as the ratio of the number of cluster hops observed per unit time divided by the number of observable clusters, i.e. the average motion frequency of individual SIA clusters.

Diffusion rates in quantum and classical phonon baths The archetypal problem of a particle traversing a potential barrier has been treated exhaustively; see Ref. [32] for a thorough review. For a barrier height $\Delta V \gg k_B T$, the classical escape rate is given by the Arrhenius function $\Gamma^{\mathrm{cl}} = f_{\mathrm{cl}} \exp(-\Delta V / k_B T)$, where the classical prefactor f_{cl} can be loosely interpreted as an attempt frequency. As $k_{\mathrm{B}} T$ rises towards ΔV the Arrhenius function breaks down, and the rate transitions to a form linear in the temperature[9,20] (manifested as a sharp steepening on an Arrhenius plot). For barriers $\Delta V \sim k_B T$ or less, the particle migrates stochastically, being slowed only by the dissipative coupling between the particle and the underlying phonon bath. This is quantified by the friction parameter γ, and the rate is proportional to $k_{\mathrm{B}} T / \gamma$ [9,20,33]. If $\Delta V \ll k_{\mathrm{B}} T$, the friction can be absorbed into f_{cl}[32,34]. Both standard rate formulae originate from the classical Boltzmann distribution for the phonons. For clusters escaping from traps, the barrier to be overcome is $\Delta V = \Delta V_{\mathrm{P}} + \Delta V_{\mathrm{trap}}$, the sum of the Peierls barrier and the critical binding energy of the impurity or vacancy respectively. Therefore the diffusion rate is the product of two independent probabilities: the probability related to the free migration of the SIA cluster through the Peierls

potential in the absence of a trap, and the escape probability from the trap itself: $\Gamma^{cl}(T) = \Gamma_P(T) \times \Gamma_{trap}(T)$. $\Delta V_{trap} \gg k_B T$, so Γ_{trap} is Arrhenius in the classical limit. Since the Peierls barrier ΔV_P for SIA clusters (a.k.a. ½⟨111⟩ loops) is small, i.e. of order $k_B T$, the total classical rate becomes:

$$\Gamma^{cl}(T) = \text{Const.} \times k_B T \times \exp\left(-\frac{\Delta V_{trap}}{k_B T}\right) \qquad (1)$$

We note that the constant prefactor above can take on a weak temperature dependence in other formulations of the rate; we obtain similar fits in either case and our conclusions are unaffected.

The full quantum-mechanical development is more complicated. Here, the Boltzmann distribution is replaced by either the Bose-Einstein (BE) or Fermi-Dirac distribution, for bosons or fermions respectively. For W or impurity atoms the ground state has integer spin and hence obeys Bose-Einstein statistic. A simple way to recover the BE phonon distribution whilst retaining the form of the classical rate formulae is to renormalize the temperature to mimic the true quantum statistics[34-36]. Consider a crystal with periodic boundary conditions represented by *N* atoms in a box. Imposing that the classical and quantum energies of the system are equal, the (renormalized, effective) classical temperature and the (true) quantum temperature should be related by the relation:

$$(3N-3)k_B T_c = \int d\omega \hbar\omega \left(\rho_{BE}(\omega, T_q) + \frac{1}{2}\right) n(\omega)$$

where T_c and T_q are the (renormalized, effective) classical and (true) quantum temperatures respectively. $n(\omega)$ is the density of states of the phonon gas, normalized to the number of modes, and $\rho_{BE}(\omega, T)$ is the BE distribution function. Therefore, the classical temperature is a function of quantum temperature $T_c = f(T_q)$.

For temperatures higher than the Debye temperature T_D, $\hbar\omega \ll k_B T$ and the energy of one oscillator becomes:

$$\hbar\omega\left(\rho_{BE}(\omega, T_q) + \frac{1}{2}\right) \approx \frac{\hbar\omega}{2} + k_B T_q \left(1 - \frac{\hbar\omega}{2k_B T_q} + \ldots\right) = k_B T_q,$$

and the classical and quantum temperatures are very close. When the (true) quantum temperature T_q tends to zero K, the effective classical temperature T_c tends to a finite limit, capturing the zero point energy:

$$(3N-3)k_{\mathrm{B}}T_c = \int \mathrm{d}\omega\, \frac{1}{2}\hbar\omega\, n(\omega)$$

The simple form $T_c = \sqrt{\tau_c^2 + T_q^2}$. satisfies these limits. Therefore, the quantum rates can be estimated by simply renormalizing the temperature in equation (1) yielding:

$$\Gamma^{\mathrm{QM}}\Gamma(T) = \text{Const.} \times k_{\mathrm{B}}\sqrt{\tau_c^2 + T^2} \times \exp\left(-\frac{\Delta V_{\mathrm{trap}}}{k_{\mathrm{B}}\sqrt{\tau_c^2 + T^2}}\right) \qquad (2)$$

Quantum TST rates

For deep tunneling, we computed the rate by numerically integrating the quantum transition state theory rate expression[34]

$$\Gamma^{\mathrm{QTST}} = (hZ_0)^{-1}\int W(E)\mathrm{e}^{-E/k_{\mathrm{B}}T}\mathrm{d}E,$$

where h is the Planck constant and $W(E)$ is the transfer integral at energy E for the sech-squared impurity interaction potential predicted by the Frenkel Kontorova model, $V^I(x_0) = \mu\Delta\mathrm{sech}^2(\mu x_0)$ ($\mu\Delta$ here corresponds to ΔV_{trap} above, see Supplementary Discussion 1). The data can be fitted with a barrier height of 55 meV, but requires an unrealistically low effective cluster mass of $m_{\mathrm{W}}/200$. The remaining parameters (potential width and curvature) are fixed by the Arrhenius limit, which applies to the highest temperature points in the dataset.

References

27 Amino, T., Arakawa, K. & Mori, H. Activation energy for long-range migration of self-interstitial atoms in tungsten obtained by direct measurement of radiation-induced point-defect clusters. *Philosophical Magazine Letters* **91**, 86-96, doi:10.1080/09500839.2010.533133 (2011).

28 Maury, F., Biget, M., Vajda, P., Lucasson, A. & Lucasson, P. Frenkel pair creation and stage I recovery in W crystals irradiated near threshold. *Radiation Effects* **38**, 53-65, doi:10.1080/00337577808233209 (1978).

29 Arakawa, K., Amino, T. & Mori, H. Direct observation of the coalescence process between nanoscale dislocation loops with different Burgers vectors. *Acta Mater* **59**, 141-145, doi:10.1016/j.actamat.2010.09.018 (2011).

30 Hirsch, P. B., Howie, A., Nicholson, R. B., Pashley, D. W. & Whelan, M. J. *Electron Microscopy of Thin Crystals*. (Butterworths, London, 1965).

31 Jenkins, M. L. & Kirk, M. A. *Characterization of Radiation Damage by Transmission Electron Microscopy*. (Institute of Physics, Bristol and Philadelphia, 2001).

32 Hänggi, P., Talkner, P. & Borkovec, M. Reaction-rate theory: fifty years after Kramers. *Reviews of Modern Physics* **62**, 251-341 (1990).

33 Dudarev, S. L. Coherent motion of interstitial defects in a crystalline material. *Philos Mag* **83**, 3577-3597, doi:10.1080/14786430310001599388 (2003).
34 Benderskii, V., Makarov, D. & Wight, C. *Chemical Dynamics at Low Temperature*. (Wiley-Interscience, 1994).
35 Wang, C. Z., Chan, C. T. & Ho, K. M. Tight-binding molecular-dynamics study of phonon anharmonic effects in silicon and diamond. *Physical Review B* **42**, 11276-11283 (1990).
36 Thomas, D. S., Pui-Wai, M. & Sergei, L. D. Low temperature diffusivity of self-interstitial defects in tungsten. *New Journal of Physics* **19**, 073024 (2017).

Figures

a

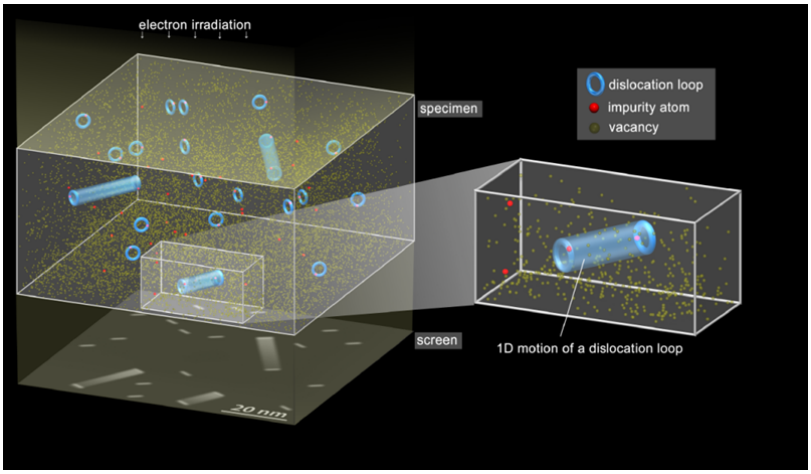

b

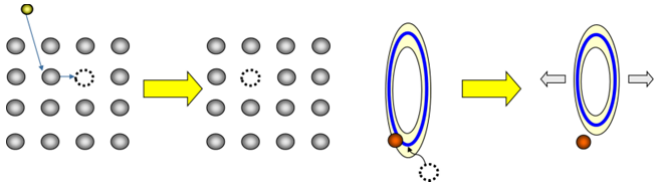

c

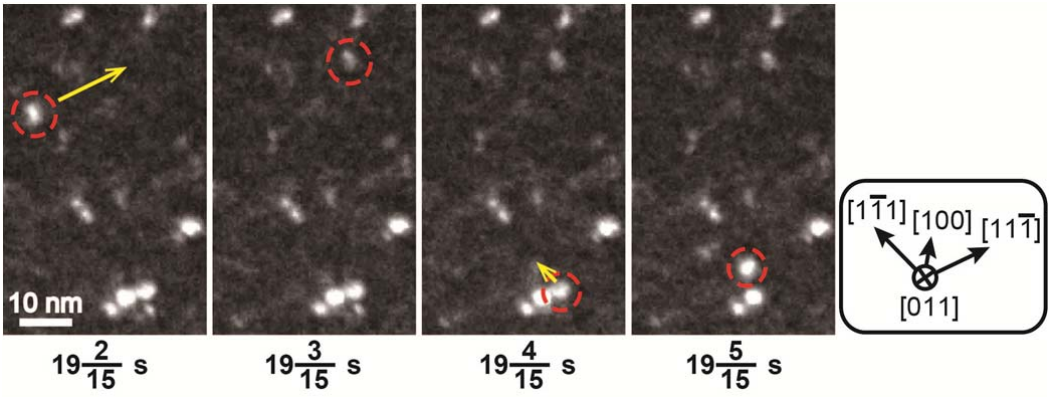

Figure 1 | 1D SIA cluster motion. a: Experimental setup. In a high-purity tungsten specimen, SIA clusters in the form of nanoscale ½⟨111⟩ dislocation loops are trapped by impurity atoms at their boundary. **b**: High-energy electron irradiation mobilizes the thermally immobile vacancies, allowing the clusters to shrink by vacancy absorption and to subsequently escape (see Supplementary Discussion 2). **c**: Escaped clusters undergo fast 1D glide diffusion before being trapped by other impurity atoms. This

1D motion was monitored simultaneously (acceleration voltage: 1000 kV; beam intensity: 2×10^{25} $m^{-2}s^{-1}$; temperature: 260 K, see Supplementary Video 1). Circled clusters move in the directions indicated by arrows, parallel to the $\frac{1}{2}\langle 111 \rangle$ type cluster Burgers vectors. The clusters hop distances of several nm to a few tens of nm within a single 1/15 s movie frame.

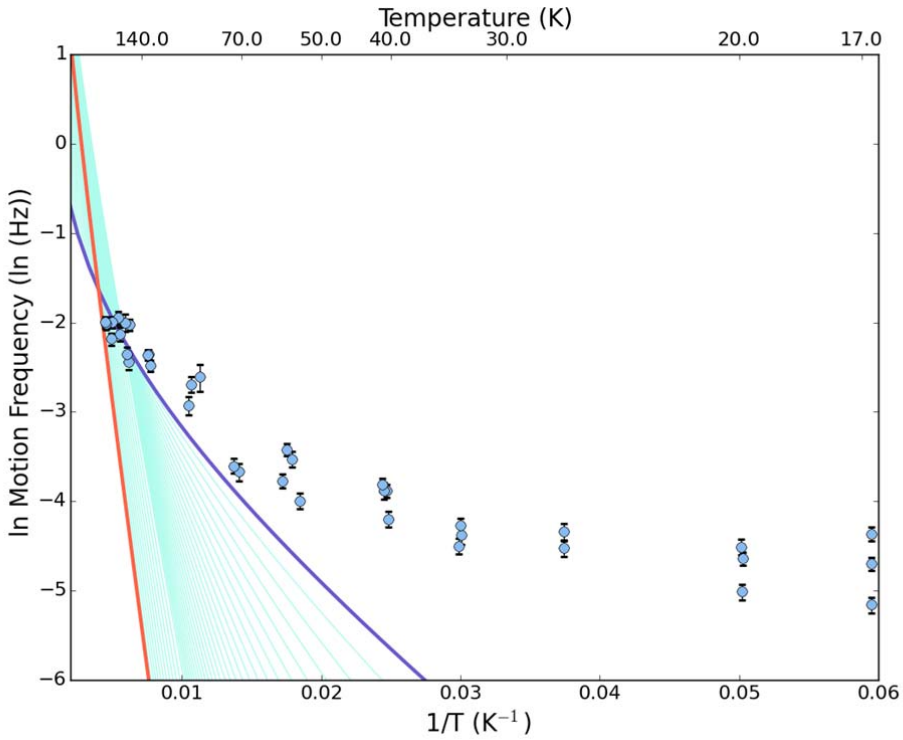

Figure 2 | **Motion frequency of SIA clusters escape.** Blue dots: motion frequency vs. temperature (conditions as Fig. 1c; data taken in first 60 s of irradiation). Some error bars are too small to be visible. Lines: all possible classical fits for activation barriers between 10 meV (blue) and 90 meV (red). Pale blue lines are intermediate values. No classical fit can capture the temperature dependence.

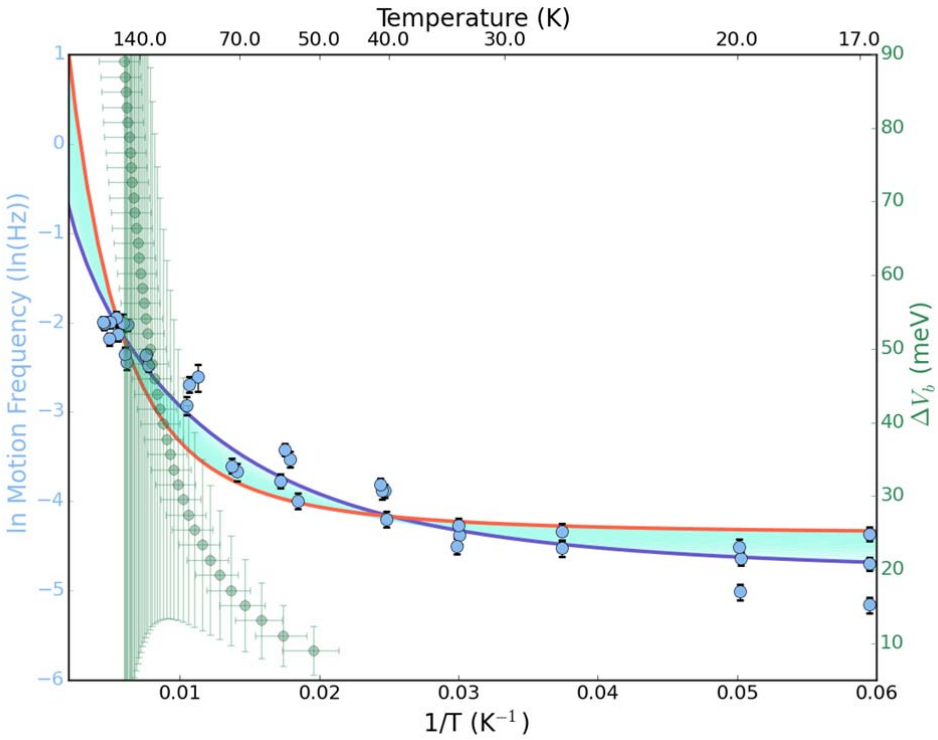

Figure 3 | **Nature of escape mechanism based on motion frequency.** Blue data points as Fig. 2. Lines: fits using quantum mechanical rate expressions for activation barriers between 10 meV (blue) and 90 meV (red). Pale blue lines are intermediate values (see Methods). Green points: fitted correlation between activation barrier and critical temperature T_c (see text), with corresponding errors bars.

Extended Display Items

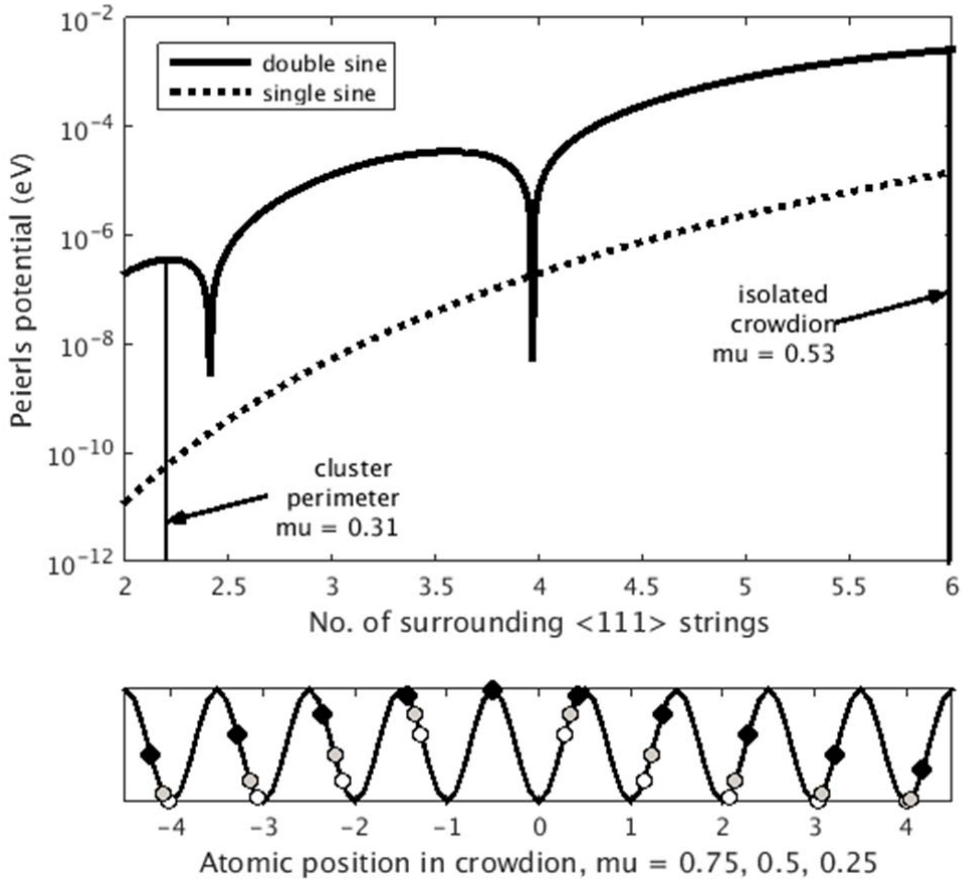

Extended Data Figure 1 | Top: suppression of Peierls potential as delocalization increases (and μ decreases). Both the standard single-sine and more accurate double-sine Frenkel-Kontorova models predict a negligibly small barrier for cluster diffusion after escape from the traps. Bottom: atomic positions showing increased delocalization as μ decreases from 0.75 (open circles) through 0.5 (grey circles) to 0.25 (solid circles).

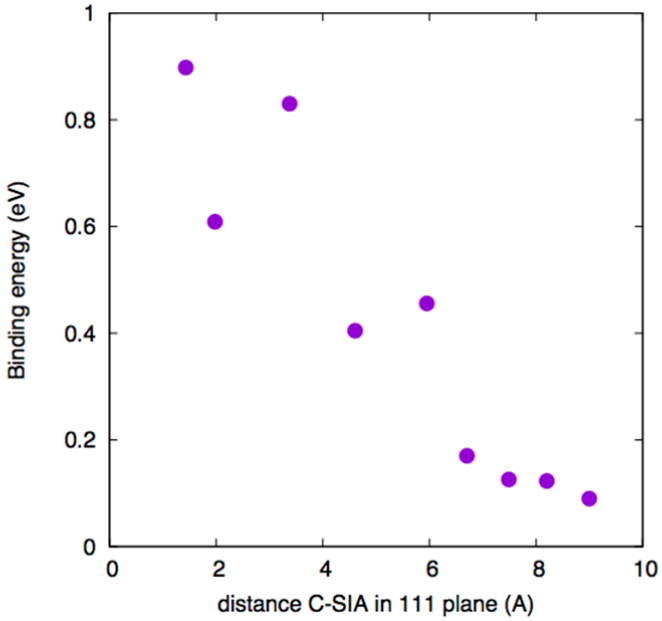

458

459 **Extended Data Figure 2a |** DFT calculation of the SIA-carbon binding energy vs.
460 separation in plane transverse to the crowdion axis.

461

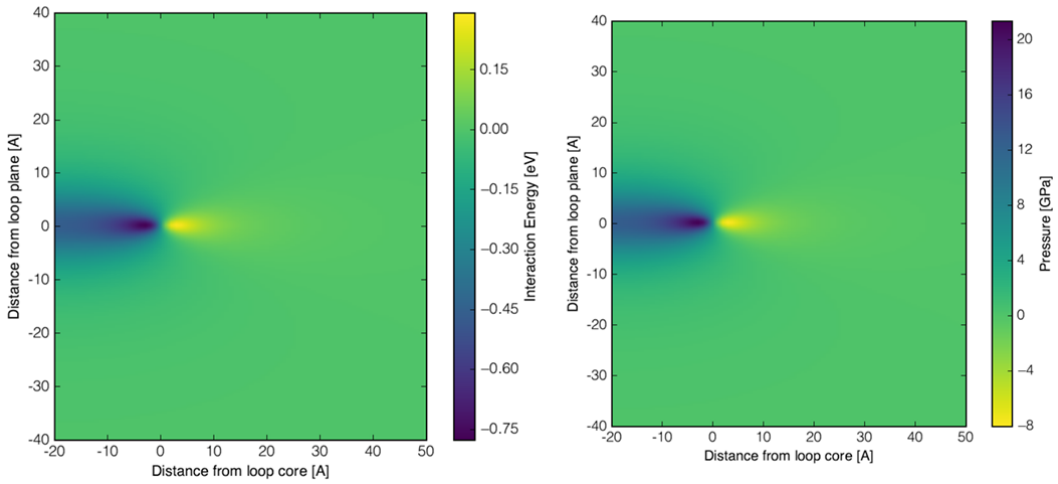

462

463 **Extended Data Figure 2b |** Elastic calculation of the SIA cluster-vacancy binding
464 energy (left) and cluster pressure field (right).

465

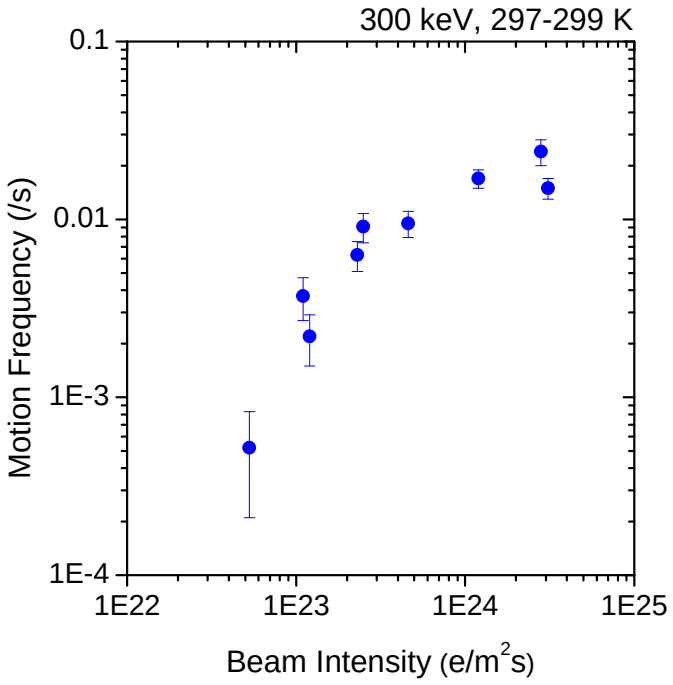

466

467 **Extended Data Figure 3a |** Motion frequency increasing with beam intensity.

468

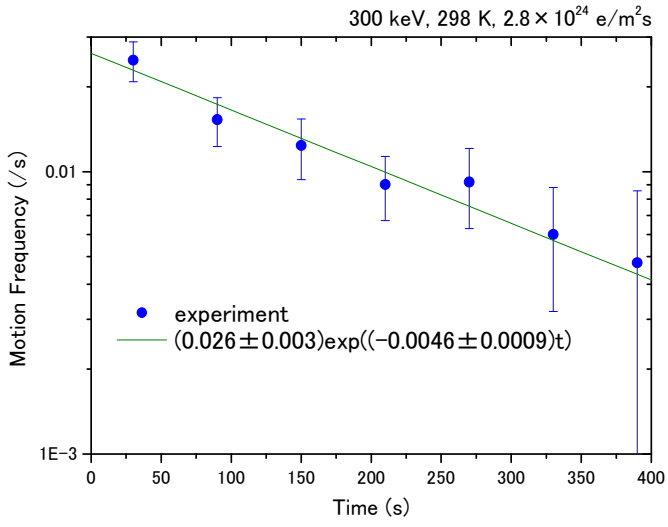

469

470 **Extended Data Figure 3b |** Motion frequency decaying exponentially with time

471 under irradiation.

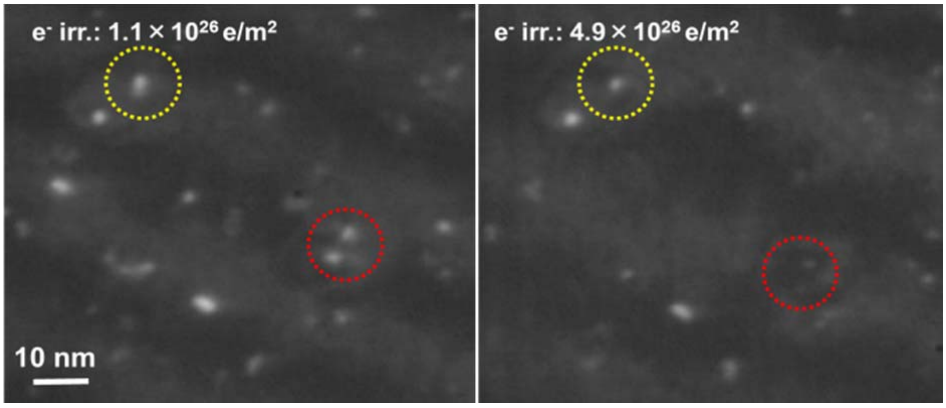

Extended Data Figure 3c | SIA cluster shrinking under the beam at 298K (vacancies are thermally immobile).

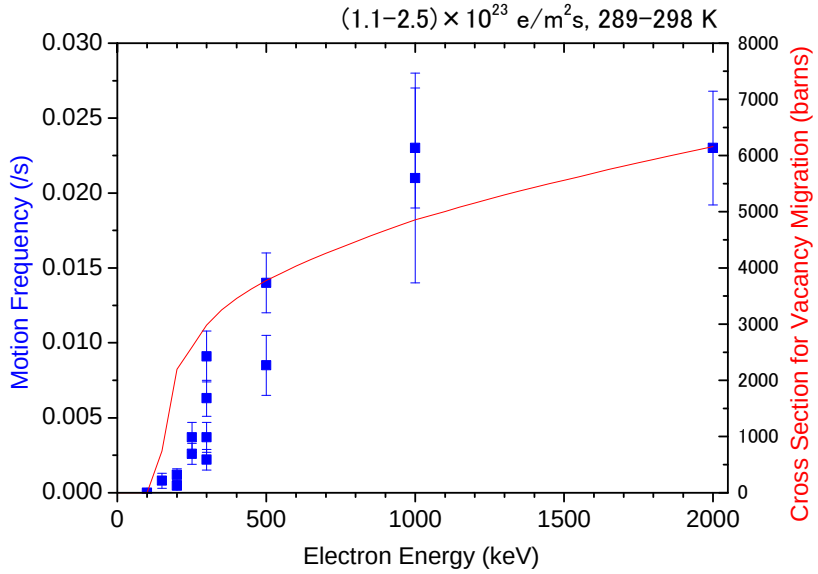

Extended Data Figure 3d | Motion frequency vs. beam energy and cross section for radiation-induced vacancy migration.

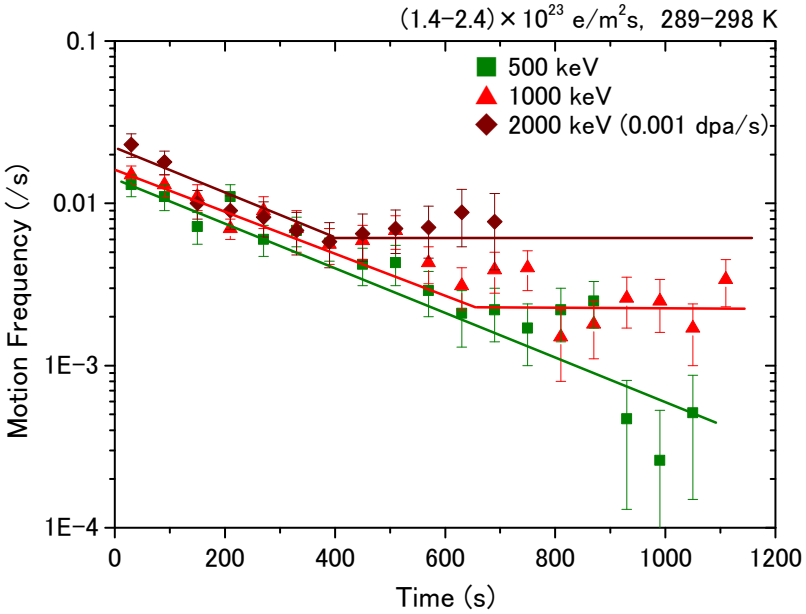

481

482 **Extended Data Figure 3e |** Long term time dependence of cluster motion frequency.
483 Plateaus are reached when the supply of vacancies local to the clusters is exhausted
484 by annihilation, and the direct mechanism takes over.

485

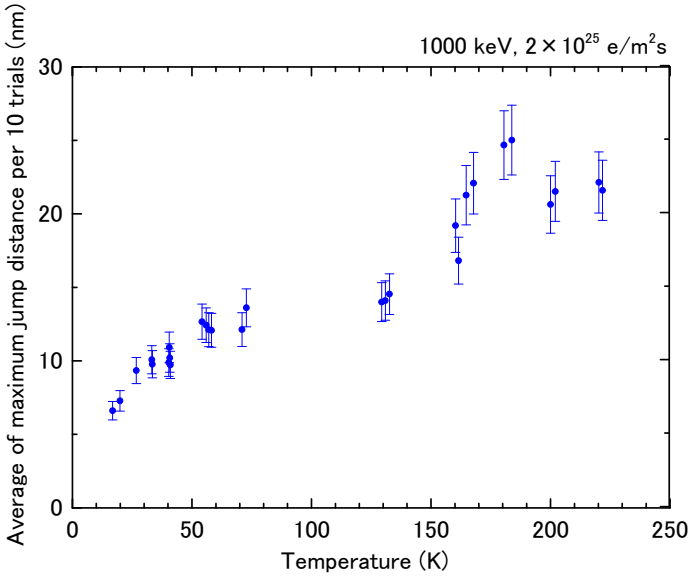

486

487 **Extended Data Figure 4 |** Average maximum hop distance per 10 hops vs
488 temperature.